



저작자표시-비영리-변경금지 2.0 대한민국

이용자는 아래의 조건을 따르는 경우에 한하여 자유롭게

- 이 저작물을 복제, 배포, 전송, 전시, 공연 및 방송할 수 있습니다.

다음과 같은 조건을 따라야 합니다:



저작자표시. 귀하는 원저작자를 표시하여야 합니다.



비영리. 귀하는 이 저작물을 영리 목적으로 이용할 수 없습니다.



변경금지. 귀하는 이 저작물을 개작, 변형 또는 가공할 수 없습니다.

- 귀하는, 이 저작물의 재이용이나 배포의 경우, 이 저작물에 적용된 이용허락조건을 명확하게 나타내어야 합니다.
- 저작권자로부터 별도의 허가를 받으면 이러한 조건들은 적용되지 않습니다.

저작권법에 따른 이용자의 권리는 위의 내용에 의하여 영향을 받지 않습니다.

이것은 [이용허락규약\(Legal Code\)](#)을 이해하기 쉽게 요약한 것입니다.

[Disclaimer](#)

Master's Thesis

Unsupervised training of deep learning based image denoisers from undersampled measurements

Magaiya Zhussip

Department of Electrical and Computer Engineering

Graduate School of UNIST

2019

**Unsupervised training of deep learning
based image denoisers from undersampled
measurements**

Maguiya Zhussip

**Department of Electrical and Computer Engineering
Graduate School of UNIST**

Unsupervised training of deep learning based image denoisers from undersampled measurements

A thesis
submitted to the Graduate School of UNIST
in partial fulfillment of the
requirements for the degree of
Master of Science

Magaiya Zhussip

May 31, 2019
Approved by



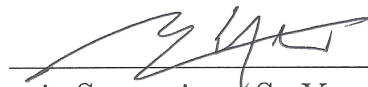
Advisor
Se Young Chun

Unsupervised training of deep learning
based image denoisers from undersampled
measurements

Magaiya Zhussip

This certifies that the thesis of Magaiya Zhussip is approved.

May 31, 2019



Thesis Supervisor: Se Young Chun



Seungjoon Yang Thesis Committee Member #1



Won-Ki Jeong: Thesis Committee Member #2

Abstract

Compressive sensing is a method to recover the original image from undersampled measurements. In order to overcome the ill-posedness of this inverse problem, image priors are used such as sparsity, minimal total-variation, or self-similarity of images. Recently, deep learning based compressive image recovery methods have been proposed and have yielded state-of-the-art performances. They used data-driven approaches instead of hand-crafted image priors to regularize ill-posed inverse problems with undersampled data. Ironically, training deep neural networks (DNNs) for them requires “clean” ground truth images, but obtaining the best quality images from undersampled data requires well-trained DNNs.

To resolve this dilemma, we propose novel methods based on two well-grounded theories: denoiser-approximate message passing (D-AMP) and Stein’s unbiased risk estimator (SURE). Our proposed methods, LDAMP SURE and LDAMP SURE-T, were able to train deep learning based image denoisers from undersampled measurements without ground truth images and without additional image priors and to recover images with state-of-the-art qualities from undersampled data. We evaluated our methods for various compressive sensing recovery problems with Gaussian random, coded diffraction pattern, and compressive sensing MRI (CS-MRI) measurement matrices. Our proposed methods yielded state-of-the-art performances for all cases without ground truth images. Our methods also yielded comparable performances to the approaches with ground truth data. Moreover, we have extended our methods to deal with a Gaussian noise in a measurement domain and further enhance reconstruction quality by developing image refining method called LDAMP SURE-FT.

Contents

Contents	ii
List of Figures	iv
List of Tables	v
I. Introduction	1
1.1 Compressed Sensing	1
1.2 Purpose of This work	2
1.3 Organization and contribution of the Thesis	3
II. Background and Literature review	4
2.1 Compressed Sensing Theory	4
2.2 Deep learning in compressive image recovery	5
2.3 Deep learning without ground truth	5
2.4 Denoiser-based AMP (D-AMP)	6
2.5 Unsupervised training with Stein’s unbiased risk estimator	8
III. Proposed LDAMP-SURE	10
3.1 Methodology	10
3.1.1 Towards a single denoiser	10
3.1.2 Unsupervised DNN training from CS measurement data	11
3.1.3 Noise estimation accuracy for MC-SURE based denoiser learning	12
3.2 Simulation Results	15
3.2.1 Experimental Setup	15
3.2.1.1 Datasets	15
3.2.1.2 Initialization of DnCNN denoiser	15
3.2.1.3 Training LDAMP SURE	16
3.2.2 Results on various measurement matrices	17
3.2.2.1 Gaussian measurement matrix	17

3.2.2.2	Coded diffraction pattern measurements	19
3.2.2.3	CS MR measurement matrix	21
3.3	Extensions	23
3.3.1	Extension to a noisy measurement data	23
3.3.2	Unsupervised fine-tuning using MC-SURE	24
IV.	Conclusion	26
	References	28

List of Figures

1.1	Applications of Compressed Sensing: (a) MR scanning, (b) Radar imaging, (c) Single pixel camera at Rice University [1], (d) Coded-aperture imaging, (e) Hyperspectral image blocks.	2
2.1	Approaches to train deep learning based denoisers with ground truth images (supervised, top), with noisy images or pairs of noisy images (unsupervised, middle), and with undersampled CS measurements (unsupervised, bottom).	7
3.1	Normalized residual histograms of “Boat” image after 10 iterations using LDAMP-BM3D for CDP matrix. Normalization was done with estimated sigma from (a) true residual (b) \mathbf{z}_T (D-AMP) and (c) $\text{Re}(\mathbf{A}^H \mathbf{z}_T)$ (Proposed).	14
3.2	Reconstructions of 180×180 test image with i.i.d. Gaussian matrix with $M/N = 0.25$ sampling rate.	18
3.3	Reconstructions of 180×180 test image with CDP measurement matrix for $M/N = 0.15$ sampling rate.	20
3.4	Reconstructions of 180×180 test image with CS-MRI measurement matrix for $M/N = 0.40$ sampling rate. Residual errors are shown in red boxes.	22

List of Tables

3.1	Performance of LDAMP networks on 100 test images with 180×180 for $M/N = 25\%$ sampling rate.	11
3.2	Average PSNR of 100 images of four different methods including our proposed method for CDP measurements.	14
3.3	Average PSNRs (dB) and run times (sec) of 100 180×180 image reconstructions for <i>i.i.d.</i> Gaussian measurements case (no measurement noise) at various sampling rates ($M/N \times 100\%$).	17
3.4	Average PSNRs (dB) and run times (sec) of 100 180×180 image reconstructions for CDP measurements case (no measurement noise) at various sampling rates ($M/N \times 100\%$).	19
3.5	Average PSNRs of 100 test images with 180×180 reconstructed for CDP at $M/N = 5\%$	20
3.6	Average PSNRs (dB) and run times (sec) of 100 180×180 image reconstructions for CS-MRI measurements case (no measurement noise) at various sampling rates ($M/N \times 100\%$).	21
3.7	Average PSNRs (dB) and run times (sec) of 100 180×180 image reconstructions for Gaussian measurements case and observation noise with $\text{SNR} = -20$ dB at various sampling rates.	23
3.8	Results of image reconstruction methods on Set 12 (256×256) for various sampling rates (Performance in dB).	25

Acknowledgement

During my master's degree at UNIST, I had a chance to meet and interact with many talented and dedicated people with a great passion inside. Using this opportunity, I would like to thank them.

First, I wish to express sincere gratitude and deep appreciation to my thesis advisor, Professor Se Young Chun, for his extensive support and guidance. The office doors of Prof. Se Young Chun was always open and he was ready to help with any questions, which were raised many times throughout my master's degree. Without his valuable help, it would be impossible to complete my research work on time and gain invaluable experience. I would also like to express my sincere thanks to Professor Seungjoon Yang and Professor Won-Ki Jeong for serving as committee members in my thesis defense and their constructive comments. Without their passionate participation and encouragement, this thesis would not be successfully completed and approved.

Second, I want to say thanks to my lab mates: Hanvit Kim, Dong-Won Park, Ji-Soo Kim, Kwan-Young Kim, Won Jae Hong, Dong-Un Kang, Yong Hyeok Seo, and Hae-Soo Eun and to my friends at UNIST from "Happy, Lucky, Lazy ..." group. Moreover, I would like to thank my friends from "Tamak" community for their support even if they are far away. Thank you Anna Kim for your C support and ∞ patience.

In the end, I wish to express my very profound gratitude to my parents for providing me with unfailing support and continuous motivation throughout my MSc journey and through the process of doing this thesis.

Introduction

1.1 Compressed Sensing

Over the past decade, compressed sensing theory also known as compressive sampling (CS) drew great attention in many practical applications, because of its ability to sample and reconstruct a signal at a significantly lower rate than Nyquist sampling theory states. This novel acquisition technique demonstrated that by exploiting redundancy in a signal, one can sample and perform compression simultaneously. Consequently, CS enables fast data acquisition and eases the need for large memory space, making it attractive for a wide range of applications, including accelerated magnetic resonance imaging (MRI) [2–4], radar imaging [1, 5], single-pixel imaging [6, 7], CT [8], hyperspectral imaging [9, 10], and coded aperture imaging [11, 12]. Moreover, CS applications have been investigated extensively and now some systems are commercialized for practical usages such as low-dose CT and accelerated CS-MRI (see Figure 1.1).

Compressed sensing allows us to significantly shorten the measurement acquisition time and perform image reconstruction off-device. However, estimating the original signal from under-sampled measurements is a challenging ill-posed problem that requires prior knowledge about the desired signal to solve it. Based on a signal prior types, CS reconstruction methods can be grouped into two major categories: conventional optimization based CS techniques, which mainly use hand-crafted priors [13–18] and deep learning based methods, which are based on data-driven approach [19–22].

Conventional methods usually have well-understood behavior and are based on interpretable priors, which makes them appealing to use. Although traditional methods for CS image recovery have well-proven theoretical convergence guarantees they suffer from the computational overhead, which prevents their usage for real-time applications [23].

Moreover, with the emergence of deep learning and the empirical proof of its superior performance in many computer vision tasks, data-driven CS image reconstruction methods become more and more popular. Because of its strong representation power, deep learning based image recovery networks were able to learn local as well as deep features and have established themselves as a de facto benchmark [24–26]. These deep learning based methods take advantage of potentially available high-quality training image datasets though in practice acquiring those images is very costly in some applications and usually we have a large amount of undersampled measurement data.

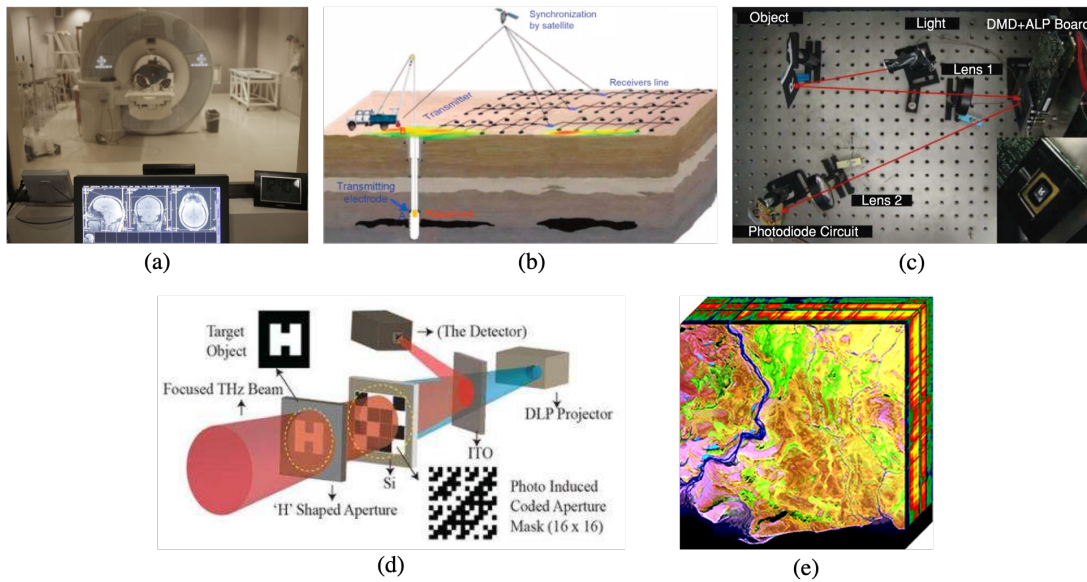


Figure 1.1: Applications of Compressed Sensing: (a) MR scanning, (b) Radar imaging, (c) Single pixel camera at Rice University [1], (d) Coded-aperture imaging, (e) Hyperspectral image blocks.

1.2 Purpose of This work

Thus, the primary aim of this paper is to investigate two main questions:

1. Can we exploit those compressively sampled measurements, which are in abundance, to train the deep learning based network for image reconstruction?
2. If yes, then to what extent it is worse/better than the deep learning based network trained on ground-truth images and traditional methods?

1.3 Organization and contribution of the Thesis

Firstly, we found that it is possible to train deep learning networks and successfully recover images from undersampled measurements. In this work, we propose unsupervised training methods for deep learning based CS image recovery based on two well-grounded theories: D-AMP and SURE. Our proposed methods were able to train DNN based image denoisers from undersampled measurements without ground truth images and to recover images with state-of-the-art qualities from undersampled data. Contributions of this work are listed below:

(1) Proposing a method to train DNN denoisers from undersampled measurements without ground truth and without additional image priors. Only one realization for each measurement was required. An accurate noise estimation method was also developed to train deep denoisers with MC-SURE.

(2) Proposing a CS image recovery method by modifying LDAMP [26] to have up to a single (or few) denoiser(s) instead of 9 denoisers with comparable performance to reduce training time.

(3) Extensive evaluations of the proposed method using high-resolution natural and MR images for the CS recovery problems with Gaussian random, coded diffraction pattern, and realistic CS MR measurement matrices.

(4) Investigating the reconstruction performance of the proposed method under the AWGN contaminated measurement data.

(5) Proposing a unsupervised fine-tuning method based on [27] for a given test CS measurement. This method often outperformed LDAMP trained with ground truth.

Secondly, the proposed approach yielded the best image recovery performance among traditional methods and in some cases was able to beat “clean” image trained networks.

It is worth to note that a part of this thesis will be presented at the 2019 IEEE/CVF Conference on Computer Vision and Pattern Recognition (CVPR) [28] and its extended version was submitted to IEEE Transactions on Image Processing (TIP) including more experiments on noisy measurements (see Chapter 3.3.1) and proposed unsupervised fine-tuning method (see Chapter 3.3.2).

This thesis is organized as follows. Chapter II reviews classical works on CS image recovery as well as state-of-the-art methods and explains two theories namely D-AMP and MC-SURE that were used as a foundation for the proposed method. In chapter III, we describe proposed LDAMP SURE, LDAMP SURE-T, and LDAMP SURE-FT algorithms in detail and evaluate its performance on different sensing matrices for various sampling rates. Finally, chapter IV draws a conclusion of this work by summarizing results and showing future directions.

Background and Literature review

2.1 Compressed Sensing Theory

Compressed Sensing (CS) or Compressive Sampling is modeled as a linear equation for the measurement:

$$\mathbf{y} = \mathbf{A}\mathbf{x} + \boldsymbol{\epsilon} \quad (\text{II.1})$$

where $\mathbf{y} \in \mathbb{R}^M$ is a measurement vector, $\mathbf{A} \in \mathbb{R}^{M \times N}$ is a sensing matrix with $M \ll N$, $\mathbf{x} \in \mathbb{R}^N$ is an unknown signal to reconstruct, and $\boldsymbol{\epsilon} \in \mathbb{R}^M$ is a noise vector. It is a challenging ill-posed inverse problem to estimate \mathbf{x} from the undersampled measurements \mathbf{y} with $M \ll N$.

Sparsity has been investigated as prior to regularize the ill-posed problem of CS recovery. CS theories allow to use l_1 norm for good signal recovery instead of l_0 norm [15, 16]. Minimizing l_1 norm is advantageous for large-scale inverse problems since l_1 norm is convex so that conventional convex optimization can be used. There have been many convex optimization algorithms for solving CS recovery problems with non-differentiable l_1 norm such as iterative shrinkage-thresholding algorithm (ISTA) [13], a fast iterative shrinkage-thresholding algorithm (FISTA) [14], alternating direction minimization (ADM) [17], and approximate message passing (AMP) [29], to name a few.

The signal \mathbf{x} itself is not usually sparse, but a transformed signal is often sparse. Signal-s/images are sparse in the wavelet domain and/or discrete cosine transform (DCT) domain. In high-resolution imaging, images have sparse edges that are often promoted by minimizing total

variation (TV) [30]. Sparse MR image recovery used both wavelet and TV priors [2] or dictionary learning prior from highly undersampled measurements [3]. Similarly, CS color video and depth recovery used both wavelet and DCT [31]. Hyperspectral imaging utilized manifold-structured sparsity prior [9] or reweighted Laplace prior [10]. Self-similarity is also used for CS image recovery such as NLR-CS [32] and denoiser-AMP (D-AMP) [23]. D-AMP utilized powerful modern denoisers such as BM3D [33] and has recently been extended to sparse MRI [34].

2.2 Deep learning in compressive image recovery

Deep learning with massive amount of data has revolutionized many computer vision tasks [35]. It has also influenced many low level computer vision tasks such as image denoising [36–41] and CS recovery [20, 25, 26, 42–45]. There are largely two different approaches using deep neural networks (DNNs) for CS recovery. One is to use a deep network to directly map from an initially recovered low-quality image from compressive samples to a high-quality ground truth image [20, 43]. The other approach for deep learning based CS image recovery is to use DNN structures that unfold optimization algorithms and learned image priors, inspired by learned ISTA (LISTA) [19]. In sparse MRI, ADMM-Net [24] and variational network [42] were proposed with excellent performances. Both methods learned parametrized shrinkage functions as well as transformation operators for sparse representation from training data. Recently, instead of using explicit parametrization in shrinkage operator, DNNs were used to unfold optimizations for CS recovery such as learned D-AMP (LDAMP) [26], ISTA-Net [45], CNN-projected gradient descent for CT [25], and Laplacian pyramid reconstructive adversarial network [44]. Utilizing generative adversarial network (GAN) for CS was also investigated [46]. These methods have one important requirement: “clean” ground truth images must be available for training.

2.3 Deep learning without ground truth

One of the most important factors for the success of deep learning based data-driven approaches in CS recovery is the availability of high quality ground truth images. Unfortunately, obtaining such ground truth images is often challenging or infeasible for the case that one desires undersampled compressive measurements. It is often expensive or infeasible to acquire clean data, for example, in medical imaging (long acquisition for MR, high radiation dose for CT) or airborne hyperspectral imaging. Thus, ironically, training DNNs requires “clean” ground truth images, while obtaining the best quality images from undersampled data requires well-trained DNNs.

Recently, there have been a few attempts to train DNNs for low-level computer vision tasks in unsupervised ways. Lehtinen *et al.* proposed noise2noise to train DNNs for image denoising, inpainting, and MR reconstruction [47]. This work was able to train DNN denoisers with two contaminated data for each image. However, applying noise2noise to more general CS applications does not seem straightforward and obtaining two independent realizations per each image may not be possible in some cases. Bora *et al.* proposed AmbientGAN, a training method for GAN with contaminated images and applied it to CS recovery [46, 48]. However, AmbientGAN was trained with artificially contaminated images, rather than with CS measurements. Moreover, the method of [46] is limited to *i.i.d.* Gaussian matrix theoretically and was evaluated with relatively low-resolution images. Soltanayev *et al.* proposed a Stein’s unbiased risk estimator (SURE) based training method for deep learning based denoisers [49]. This method requires only one noise realization, but it is limited to *i.i.d.* Gaussian noise. Moreover, it is not straightforward to extend this work to CS image recovery problems.

It is worth noting that Metzler *et al.* concurrently proposed unsupervised training methods with CS measurements and investigated a number of different theoretical approaches [50]. One of the methods in the work of Metzler applied MC-SURE and LDAMP to approximate the MSE in measurement domain and evaluated only with 6 standard test images, a CDP with 20% sampling ratio, and unit variance complex Gaussian measurement noise, while our proposed methods applied MC-SURE to approximate the MSE in image domain inside LDAMP and were investigated with much more cases and test images. LDAMP SURE in [50] was not able to outperform BM3D-AMP (30.9dB vs. 31.5dB) as well as LDAMP with ground truth (32.7dB), while our proposed methods outperformed BM3D-AMP for all cases and often outperformed LDAMP with ground truth using fine-tuning.

The summary of existing approaches for training DNN denoisers are illustrated in Fig. 2.1 (top, middle). The primary difference between them and our proposed (see in Fig. 2.1 (bottom)) methods is that image denoisers were trained with CS measurements.

2.4 Denoiser-based AMP (D-AMP)

D-AMP is an algorithm designed to solve CS problems where one needs to recover image vector \mathbf{x} from the set of measurements \mathbf{y} using prior information about \mathbf{x} . Based on the model (II.1), the problem can be formulated as:

$$\min_{\mathbf{x}} \|\mathbf{y} - \mathbf{A}\mathbf{x}\|_2^2 \quad \text{subject to} \quad \mathbf{x} \in C \quad (\text{II.2})$$

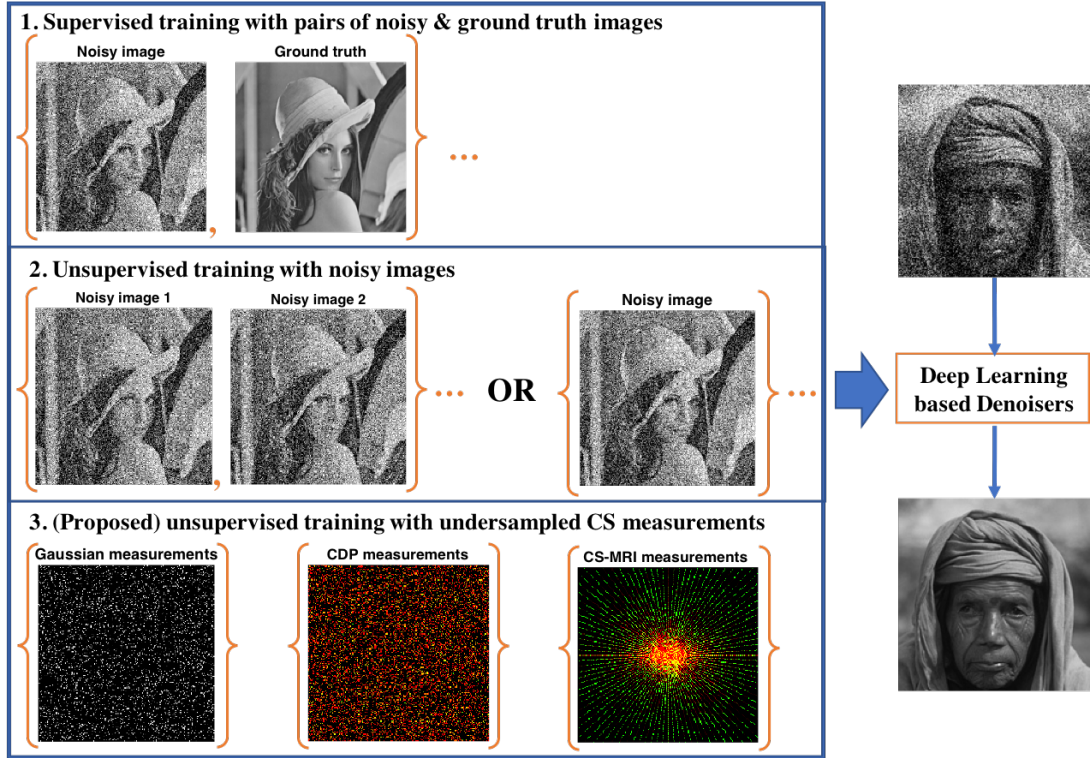


Figure 2.1: Approaches to train deep learning based denoisers with ground truth images (supervised, top), with noisy images or pairs of noisy images (unsupervised, middle), and with undersampled CS measurements (unsupervised, bottom).

where C is the set of natural images. D-AMP solves (II.2) relying on approximate message passing (AMP) theory. It employs appropriate Onsager correction term \mathbf{b}_t at each iteration, so that $\mathbf{x}_t + \mathbf{A}^H \mathbf{z}_t$ in Algorithm 1 becomes close to the ground truth image plus *i.i.d.* Gaussian noise. D-AMP can utilize any denoiser as a mapping operator $\mathbf{D}_{\mathbf{w}(\hat{\sigma}_t)}(\cdot)$ in CS recovery (Algorithm 1) for reducing *i.i.d.* Gaussian noise as far as the divergence of denoiser can be obtained.

D-AMP [51] first utilized conventional state-of-the-art denoisers such as BM3D [33] for $\mathbf{D}_{\mathbf{w}(\hat{\sigma}_t)}(\cdot)$ in Algorithm 1. Given a standard deviation of noise $\hat{\sigma}_t$ at iteration t , BM3D was applied to a noisy image $\mathbf{x}_t + \mathbf{A}^H \mathbf{z}_t$ to yield estimated image \mathbf{x}_{t+1} . Since BM3D can not be represented as a linear function, analytical form for divergence of this denoiser is not available for obtaining Onsager term. This issue was resolved by using Monte-Carlo (MC) approximation for divergence term $\text{div} \mathbf{D}_{\mathbf{w}(\hat{\sigma}_t)}(\cdot)$ [52]: For $\epsilon > 0$ and $\tilde{\mathbf{n}}$ is a standard normal random vector,

$$\text{div} \mathbf{D}_{\mathbf{w}(\hat{\sigma}_t)}(\cdot) \approx \frac{\tilde{\mathbf{n}}'}{\epsilon} (\mathbf{D}_{\mathbf{w}(\hat{\sigma}_t)}(\cdot + \epsilon \tilde{\mathbf{n}}) - \mathbf{D}_{\mathbf{w}(\hat{\sigma}_t)}(\cdot)). \quad (\text{II.3})$$

Recently, LDAMP [26] was proposed to use deep learning based denoisers for $\mathbf{D}_{\mathbf{w}(\hat{\sigma}_t)}(\cdot)$ in

Algorithm 1. Nine DNN denoisers were trained with noiseless ground truth data for different noise levels. LDAMP consists of 10 D-AMP layers (iterations) and DnCNN [40] was used in each layer as a denoiser operator. Unlike other unrolled neural network versions of iterative algorithms such as learned-AMP [53] and LISTA [19], LDAMP exploited imaging system models, which are fixed \mathbf{A} and \mathbf{A}^H operators while the parameters for DnCNN denoisers were trained with ground truth data in the image domain.

Algorithm 1 (Learned) D-AMP algorithm [23, 26]

1: Signal initialization $\mathbf{x}_0 = \mathbf{0}, \mathbf{y}, \mathbf{A}$

2: **for** $t = 0$ to T **do**

3: Update Onsager correction term:

$$\mathbf{b}_t = \mathbf{z}_{t-1} \operatorname{div} \mathbf{D}_{\mathbf{w}(\hat{\sigma}_{t-1})}(\mathbf{x}_{t-1} + \mathbf{A}^H \mathbf{z}_{t-1}) / M$$

4: Calculate the residual in measurement domain:

$$\mathbf{z}_t = \mathbf{y} - \mathbf{A} \mathbf{x}_t + \mathbf{b}_t$$

5: Estimate signal noise standard deviation:

$$\hat{\sigma}_t = \|\mathbf{z}_t\|_2 / \sqrt{M}$$

6: Estimate the reconstructed signal by denoising noisy image:

$$\mathbf{x}_{t+1} = \mathbf{D}_{\mathbf{w}(\hat{\sigma}_t)}(\mathbf{x}_t + \mathbf{A}^H \mathbf{z}_t)$$

7: **end for**

8: Final reconstructed signal: \mathbf{x}_T

2.5 Unsupervised training with Stein’s unbiased risk estimator

Over the past years, DNN based denoisers have been well investigated [36–41] and often outperformed conventional denoisers such as BM3D [33] and non-local filtering [54, 55]. DNN denoisers such as DnCNN [40] yielded state-of-the-art denoising performance at multiple noise levels and are typically trained by minimizing the mean square error (MSE) between the output

image of denoiser and the noiseless ground truth image:

$$\frac{1}{K} \sum_{j=1}^K \|\mathbf{D}_{\mathbf{w}(\sigma)}(\mathbf{z}^{(j)}) - \mathbf{x}^{(j)}\|^2 \tag{II.4}$$

where $\mathbf{z} \in \mathbb{R}^N$ is a noisy image of the ground truth image \mathbf{x} contaminated with *i.i.d.* Gaussian noise with zero mean and fixed σ^2 variance, $\mathbf{D}_{\mathbf{w}(\sigma)}(\cdot)$ is a deep learning based denoiser with large-scale parameters \mathbf{w} to train, and $(\mathbf{z}^{(1)}, \mathbf{x}^{(1)}), \dots, (\mathbf{z}^{(K)}, \mathbf{x}^{(K)})$ is a training dataset with K samples in image domain.

Recently, a method to train deep learning based denoisers only with noisy images was proposed [49]. Instead of minimizing MSE, the following Monte-Carlo Stein’s unbiased risk estimator (MC-SURE) of MSE was minimized with respect to large-scale weights \mathbf{w} in the DNN without noiseless ground truth images:

$$\frac{1}{K} \sum_{j=1}^K \|\mathbf{z}^{(j)} - \mathbf{D}_{\mathbf{w}(\sigma)}(\mathbf{z}^{(j)})\|^2 - N\sigma^2 + \frac{2\sigma^2\tilde{\mathbf{n}}'}{\epsilon} \left(\mathbf{D}_{\mathbf{w}(\sigma)}(\mathbf{z}^{(j)} + \epsilon\tilde{\mathbf{n}}) - \mathbf{D}_{\mathbf{w}(\sigma)}(\mathbf{z}^{(j)}) \right). \tag{II.5}$$

In compressive image recovery applications, there are often cases where no ground truth data or no Gaussian contaminated images are available, but only compressive samples in measurement domain are available for training. However, it is not straightforward to use MSE or MC-SURE based deep denoiser networks for CS image recovery unless additional image priors are used. The goal of this article is to propose a method to train DNN denoisers directly from compressive samples without additional image prior and to simultaneously recover images.

Proposed LDAMP-SURE

In this chapter, we first explain the proposed methods in details and try to optimize the LDAMP network by reducing the number of deep denoisers in it without losing much performance. Then, we prove the importance of the estimated noise accuracy for MC-SURE performance. Finally, several experiments for different measurement matrices are conducted to verify the effectiveness of our approach.

3.1 Methodology

3.1.1 Towards a single denoiser

The original LDAMP utilized 9 DnCNN denoisers trained on “clean” images for different noise levels ($\sigma = 0-10, 10-20, 20-40, 40-60, 60-80, 80-100, 100-150, 150-300, 300-500$). However, we argue that training a single DnCNN denoiser is often enough to achieve almost the same performance.

Extensive studies have been performed to understand how the number of denoisers can affect the performance of LDAMP network with the goal of reducing the number of denoisers from 9 [26] to 1 or more without losing much performance. All networks were trained on BSD-500 dataset and with a MSE as a loss function. The results are tabulated in Table 3.1, where the number indicates the number of denoisers in LDAMP. For instance, LDAMP-3 means LDAMP with 3 DnCNN denoisers trained on noise ranges specified in the “Trained noise range” column.

It turned out that the more number of DnCNN denoisers and the finer discretization of the noise range are used, the better performance of the LDAMP.

On the other hand, we found that the hybrid approach using LDAMP-1 and BM3D could achieve comparable performance with only 1 DnCNN. When we utilized state-of-the-art BM3D denoiser for larger noise levels and use one blind DnCNN at low noise range, comparable reconstruction performance to LDAMP-9 was able to be achieved. This reduces network training time significantly.

Table 3.1: Performance of LDAMP networks on 100 test images with 180×180 for $M/N = 25\%$ sampling rate.

Networks	Gaussian	CDP	CS-MRI	Trained noise range
LDAMP-9 [26]	31.30	35.07	31.41	$\sigma \in [0 - 10, 10 - 20, \dots, 300 - 500]$
LDAMP-4	31.19	32.84	29.64	$\sigma \in [0 - 50, \dots, 200 - 500]$
LDAMP-3	31.35	32.96	29.42	$\sigma \in [0 - 50, 50 - 150, 150 - 500]$
LDAMP-3	30.92	33.06	29.47	$\sigma \in [0 - 100, 100 - 200, 200 - 500]$
LDAMP-1	28.45	31.00	28.56	$\sigma \in [0 - 500]$
LDAMP w BM3D	31.65	33.88	31.33	$\sigma \in [0 - 55]$ and BM3D for larger noise

3.1.2 Unsupervised DNN training from CS measurement data

Our proposed method exploits D-AMP (LDAMP) [23, 26] to yield Gaussian noise contaminated image estimates during compressive image recovery from large-scale undersampled measurements and to train a single DNN denoiser with these noisy estimates at different noise levels using MC-SURE based denoiser learning [49]. Since Onsager correction term in D-AMP makes $\mathbf{x} + \mathbf{A}^H \mathbf{z}$ term to be close to the ground truth image plus Gaussian noise, we conjecture that these can be utilized for MC-SURE based denoiser training. Our joint algorithm is detailed in Algorithm 1. Note that for large-scale CS measurements $\mathbf{y}^{(1)}, \dots, \mathbf{y}^{(K)}$, both images $\hat{\mathbf{x}}_L^{(1)}, \dots, \hat{\mathbf{x}}_L^{(K)}$ and trained denoising DNN $\mathbf{D}_{\mathbf{w}_L(\sigma)}(\cdot)$ were able to be obtained. After training, fast and high performance CS image recovery was possible without further training of denoising DNN.

Firstly, we propose to pre-train a DnCNN network for the standard deviation of $\sigma \in [0, 55]$ with the reconstructed images using BM3D-AMP as ground truth and with additive Gaussian noise. Then, our proposed Algorithm 1 generates denoised image estimate \mathbf{x}_{t+1} using pre-trained DnCNN blind denoiser $\mathbf{D}_{\mathbf{w}_t(\hat{\sigma}_t)}$ with $\mathbf{x}_t + \mathbf{A}^H \mathbf{z}_t$ for the noise level between $[0, 55]$ (line 10 in Algorithm 1) or using BM3D filter $BM3D_{\hat{\sigma}_t}$ for higher level noise reduction (line 12 in

Algorithm 1). Depending on a sampling ratio and forward operator \mathbf{A} , initial 2-4 iterations are usually utilized BM3D to decrease the noise level that is sufficient enough for using blind DnCNN. After T iterations, the set of training data $\mathbf{s}_l^{(1)}, \dots, \mathbf{s}_l^{(K)}$ can be generated and then those noisy training images were used for further training the DnCNN with MC-SURE.

Note that the noise level range for DnCNN is subject to change depending on a particular problem. For example, we found that for *i.i.d.* Gaussian and CDP matrices, training DnCNN with $\sigma \in [0, 55]$ seems to work well, while for CS MRI case, the range should be shortened to $\sigma \in [0, 10]$ for comparable results to the original 9 DnCNN denoisers.

For highly undersampled cases (e.g. $M/N = 5\%$), the noise range of a single DnCNN denoiser was extended to $\sigma \in [0, 80]$ for Gaussian sensing matrices. However, for CDP matrices, using more denoisers was necessary to maintain the performance. Thus, we used three blind DnCNN denoisers that were trained for $\sigma_1 \in [0, 55]$, $\sigma_2 \in [55, 110]$, and $\sigma_3 \in [110, 165]$ noise ranges, respectively, for $M/N = 5\%$.

3.1.3 Noise estimation accuracy for MC-SURE based denoiser learning

In D-AMP and LDAMP [23, 26], noise level was estimated in measurement domain using

$$\hat{\sigma}_t = \|\mathbf{z}_t\|_2 / \sqrt{M}. \quad (\text{III.1})$$

The accuracy of this estimation was not critical for D-AMP or LDAMP since denoisers in both methods were not sensitive to different noise levels. However, accurate noise level estimation was quite important for MC-SURE based deep denoiser network learning. We investigated the accuracy of (III.1). It turned out that the accuracy of noise level estimation depends on measurement matrices.

With *i.i.d.* Gaussian measurement matrix \mathbf{A} , (III.1) was very accurate and comparable to the ground truth standard deviation that was obtained from the true residual $(\mathbf{x}_t + \mathbf{A}^H \mathbf{z}_t) - \mathbf{x}_{true}$. However, with coded diffraction pattern measurement matrix \mathbf{A} that yields complex measurements, it turned out that (III.1) yielded over-estimated noise level for multiple examples. Since the image \mathbf{x}_t is real, we propose a new standard estimation method for D-AMP:

$$\hat{\sigma}_t = \|\text{Re}(\mathbf{A}^H \mathbf{z}_t)\|_2 / \sqrt{N}. \quad (\text{III.2})$$

Algorithm 2 Simultaneous LDAMP and MC-SURE deep denoiser learning algorithm

- 1: Input the set of measurements and sensing matrix: $\mathbf{y}^{(1)}, \dots, \mathbf{y}^{(K)}, \mathbf{A}$
- 2: **for** $l = 1$ to L **do**
- 3: **for** $k = 1$ to K **do**
- 4: **for** $t = 0$ to T **do**
- 5: Update Onsager correction term:

$$\mathbf{b}_t = \mathbf{z}_{t-1} \text{div} \mathbf{D}_{w_l(\hat{\sigma}_{t-1})}(\mathbf{x}_{t-1} + \mathbf{A}^H \mathbf{z}_{t-1}) / M$$

- 6: Calculate the residual in measurement domain:

$$\mathbf{z}_t = \mathbf{y}^{(k)} - \mathbf{A} \mathbf{x}_t + \mathbf{b}_t$$

- 7: Estimate signal noise standard deviation:

$$\hat{\sigma}_t = \|\mathbf{z}_t\|_2 / \sqrt{M}$$

- 8: Estimate the reconstructed signal by denoising noisy image:

- 9: **if** $\hat{\sigma}_t \leq 55$. **then**

- 10: $\mathbf{x}_{t+1} = \mathbf{D}_{w_l(\hat{\sigma}_t)}(\mathbf{x}_t + \mathbf{A}^H \mathbf{z}_t)$

- 11: **else**

- 12: $\mathbf{x}_{t+1} = \text{BM3D}_{\hat{\sigma}_t}(\mathbf{x}_t + \mathbf{A}^H \mathbf{z}_t)$

- 13: **end if**

- 14: **end for**

- 15: Saving reconstructed image and pseudo data:

$$\hat{\mathbf{x}}_l^{(k)} = \mathbf{x}_{T+1}$$

$$\mathbf{s}_l^{(k)} = \mathbf{x}_T + \mathbf{A}^H \mathbf{z}_T$$

- 16: **end for**

- 17: Train $\mathbf{D}_{w_l(\sigma)}(\cdot)$ with $\mathbf{s}_l^{(1)}, \dots, \mathbf{s}_l^{(K)}$ at different noise levels σ

- 18: **end for**

- 19: Return reconstructed image and trained denoiser: $\hat{\mathbf{x}}_L^{(1)}, \dots, \hat{\mathbf{x}}_L^{(K)}, \mathbf{D}_{w_L(\sigma)}(\cdot)$
-

We performed comparison studies between (III.1), (III.2), and the ground truth from true residual $(\mathbf{x}_t + \mathbf{A}^H \mathbf{z}_t) - \mathbf{x}_{true}$ and found that they are all very similar for *i.i.d.* Gaussian measurement matrix, but our proposed method (III.2) yielded more accurate estimates of standard deviation than previous method (III.1). Figure 3.1 illustrates the accuracy of our estimator

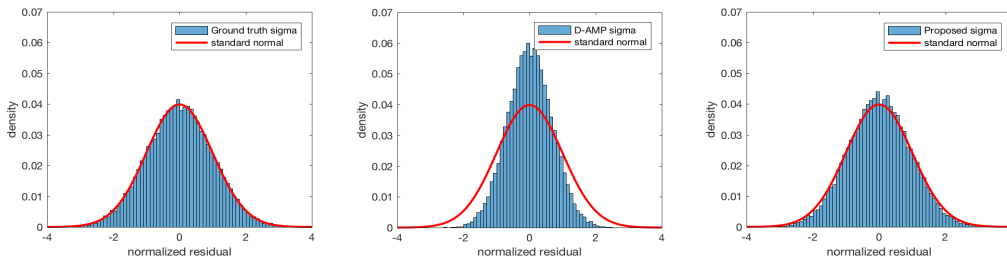


Figure 3.1: Normalized residual histograms of “Boat” image after 10 iterations using LDAMP-BM3D for CDP matrix. Normalization was done with estimated sigma from (a) true residual (b) \mathbf{z}_T (D-AMP) and (c) $\text{Re}(\mathbf{A}^H \mathbf{z}_T)$ (Proposed).

compared to previous one. When normalizing the true residual, using accurate sigma estimation yields good fitting to standard normal density (red line). Normalized histogram of true residual using ground truth and our proposed standard deviation estimation yielded good fitting to that, but the previous estimation method yielded sharper histogram, which indicates that the previous method overestimates noise level. Our proposed estimation was critical for the high performance of our proposed method with CDP measurement matrix (see Table 3.2).

Table 3.2: Average PSNR of 100 images of four different methods including our proposed method for CDP measurements.

Method	$M/N = 25\%$
BM3D-AMP [51]	31.40 dB
LDAMP BM3D	31.65 dB
LDAMP SURE w/ Proposed Noise Est.	33.26 dB
LDAMP SURE w/ Prev. Noise Est.	21.40 dB

We observed that LDAMP SURE trained with this original method yielded the worst result. Our proposed noise estimation method (Eq. (7)) significantly improved the performance of our LDAMP SURE (see Table 3.2). We compared the following four methods: BM3D-AMP [23, 51], LDAMP BM3D (the same method as [26], but trained with the results of BM3D-AMP as the ground truth using MSE), LDAMP SURE w/ Prev. Noise Est. (our proposed method, but using the previous noise estimation in [26]), and LDAMP SURE w/ Proposed Noise Est. (our proposed method with the new noise estimation). LDAMP SURE w/ Prev. Noise Est. yielded

10 dB lower than conventional BM3D-AMP, indicating that accurate noise estimation is one of the key factors for successful denoiser training using MC-SURE.

Moreover, we found out that proposed noise estimator (III.2) also can be applied to a CS-MRI case, when k-space data is not highly undersampled. Therefore, for a sampling rate of larger than 35-40%, true residual follows a Gaussian noise, which can be accurately measured by (III.2) and further utilized for training deep denoisers with MC-SURE.

3.2 Simulation Results

3.2.1 Experimental Setup

3.2.1.1 Datasets

We used images from DIV2K [56], Berkeley’s BSD-500 [57] datasets, and standard test images for training and testing our proposed method on *i.i.d.* Gaussian and CDP matrices. The training dataset was comprised of all 500 images from BSD-500, while a test set of 100 images included 75 randomly chosen images from DIV2K dataset and 25 standard test images. Since the proposed method used measurement data and fixed linear operator for image reconstruction, all test and train images had to have the same size. Thus, all images were subsampled and cropped to the size of 180×180 and then compressively sampled using the forward model \mathbf{A} to generate CS measurement data.

For CS-MRI reconstruction, Stanford dataset with 3D FSE (fast spin echo) [58] was pulled from the open repository at <http://mridata.org/>. The knee dataset included 20 patients each having 256 slices of 320×320 images. Among 20 cases of knee data, 3 cases were used for training and 1 case for testing. Images were transformed into k-space measurements and then subsampled with realistic radial sampling patterns at various sampling rates.

We implemented all methods on the Tensorflow framework and used Adam optimization [59] with the learning rate of 10^{-3} , which was dropped to 10^{-4} after 40 epochs and further trained for 10 epochs. The batch size was set to 128 and training the DnCNN denoiser took approximately 12-14 hours on one NVIDIA Titan X (Pascal).

3.2.1.2 Initialization of DnCNN denoiser

For a given measurement data \mathbf{y} from BSD-500 and linear operator \mathbf{A} , initial images were firstly reconstructed using a conventional CS recovery algorithm, BM3D-AMP. Even though the quality of these initial images was not close to the ground truth images, they still provided good pre-training data for DnCNN denoisers. Recovered images were rescaled, cropped, flipped,

and rotated to generate 298,000 image patches whose sizes are 50×50 . These patches were used as ground truth to pre-train DnCNN denoiser with MSE. Since our approach does not require dataset with ground truth, it is possible to use measurement data from the test set. Thus, we also generated 357,600 50×50 patches from reconstructed test and train images. Our DnCNN denoiser was trained for $\sigma \in [0, 55]$ noise level range with either training patches only or training and testing patches together. The former pre-trained DnCNN denoiser in the LDAMP framework is denoted by “LDAMP BM3D” and the latter pre-trained DnCNN with LDAMP is denoted by “LDAMP BM3D-T”.

BM3D-AMP-MRI was specifically tailored for CS-MRI reconstruction [34] and thus yielded significantly better results than conventional BM3D-AMP. Therefore, k-space knee dataset was reconstructed using it and then the resulted images were rescaled, cropped, flipped, and rotated to generate 267,240 and 350,320 50×50 patches for training LDAMP BM3D and LDAMP BM3D-T, respectively. We trained DnCNN denoisers for $\sigma \in [0, 10]$ noise range.

3.2.1.3 Training LDAMP SURE

Firstly, LDAMP SURE was run $T = 10$ iterations using pre-trained DnCNN denoiser and BM3D. At the last iteration, we collected images and estimated noise standard deviation with (III.2). Then, all images with noise levels in $[0, 55]$ range (CS-MRI case: $\sigma \in [0, 10]$) were grouped into one set, while images with larger noise levels were replaced by Gaussian noise added BM3D-AMP recovered images. Thus, we have the dataset of all images with $\sigma \in [0, 55]$ (CS-MRI case: $\sigma \in [0, 10]$) to train DnCNN denoiser with MC-SURE. These steps were repeated L times to further improve the performance of our proposed method. Although training DnCNN with MC-SURE involves estimation of a noise standard deviation for an entire image, we assume that a patch from an image has the same noise level as the image itself. Thus, we generated patches without using rescaling to avoid noise distortion to train LDAMP SURE.

To train DnCNN with SURE, we initialized DnCNN with the weights of pre-trained DnCNN and trained it using Adam optimizer [59] with a learning rate of 10^{-4} and batch size 128 for 10 epochs. Then, we decreased the learning rate to 10^{-5} and trained it for another 10 epochs. Training process took about 3 hours for LDAMP SURE and about 4 hours for LDAMP SURE-T. We empirically found that after $L=2$ iterations (line 3 in Algorithm 1) of training LDAMP SURE, the results converge for both CDP and *i.i.d.* Gaussian cases, while for CS-MRI, $L = 1$.

The accuracy of MC-SURE approximation depends on the selection of constant value of ϵ , which is directly proportional to σ [49, 60]. Therefore, for training DnCNN with SURE, ϵ value was calculated for each patch based on its noise level.

3.2.2 Results on various measurement matrices

3.2.2.1 Gaussian measurement matrix

We compared our proposed LDAMP SURE with the state-of-the-art CS methods that do not require ground truth data such as BM3D-AMP [51], NLR-CS [32], and TVAL3 [30]. BM3D-AMP was used with default parameters and run for 30 iterations to reduce high variation in the results, although PSNR¹ approached its maximum after 10 iterations [23]. The proposed LDAMP SURE algorithm was run 30 iterations but also showed convergence after 8-10 iterations. NLR-CS was initialized with 8 iterations of BM3D as justified in [23], while TVAL3 was set to its default parameters. We additionally reported the results of LDAMP with a single DnCNN (denoted as LDAMP MSE) that was trained on ground truth images to see the performance gap.

Table 3.3: Average PSNRs (dB) and run times (sec) of 100 180×180 image reconstructions for *i.i.d.* Gaussian measurements case (no measurement noise) at various sampling rates ($M/N \times 100\%$).

Method	Training Time	$M/N = 5\%$		$M/N = 15\%$		$M/N = 25\%$	
		PSNR	Time	PSNR	Time	PSNR	Time
TVAL3 [30]	N/A	20.46	9.71	24.14	22.96	26.77	34.87
NLR-CS [32]	N/A	21.88	128.73	27.58	312.92	31.20	452.23
BM3D-AMP [51]	N/A	21.40	25.98	26.74	24.21	30.10	23.08
LDAMP BM3D	10.90 hrs	21.41	8.98	27.54	3.94	31.20	2.89
LDAMP BM3D-T	14.30 hrs	21.42	8.98	27.61	3.94	31.32	2.89
LDAMP SURE	15.05 hrs	21.44	8.98	27.65	3.94	31.46	2.89
LDAMP SURE-T	17.97 hrs	21.68	8.98	27.84	3.94	31.66	2.89
LDAMP MSE	10.17 hrs	22.07	8.98	27.78	3.94	31.65	2.89

From Table 3.3, proposed LDAMP SURE and LDAMP SURE-T outperformed other methods at higher CS ratios by 0.26-0.46 dB, while at a highly undersampled case, it is to NLR-CS. Nevertheless, it is clear that SURE based LDAMP is able to improve the performance of pre-trained LDAMP BM3D and surpasses BM3D-AMP by 0.28-1.56 dB. In Figure 3.2, reconstructions of all methods on a test image are represented for 25% sampling ratio. Proposed LDAMP SURE and LDAMP SURE-T provide sharper edges and preserve more details.

In terms of run time, the dominant source of computation comes from using BM3D denoiser at initial iterations, while DnCNN takes less than a second for inference. LDAMP SURE utilizes

¹PSNR stands for peak signal-to-noise ratio and is calculated by following expression: $10\log_{10}\left(\frac{255^2}{\text{mean}(\hat{x}-x_{gt})^2}\right)$ for pixel range $\in [0 - 255]$

CPU for BM3D and GPU for DnCNN. Consequently, proposed LDAMP SURE was faster than BM3D-AMP, NLR-CS, and TVAL3 methods.



Figure 3.2: Reconstructions of 180×180 test image with i.i.d. Gaussian matrix with $M/N = 0.25$ sampling rate.

3.2.2.2 Coded diffraction pattern measurements

LDAMP SURE was tested with randomly sampled coded diffraction pattern [61] and yielded high-quality images retaining most structure, while details in traditionally reconstructed images were completely vanished (see Figure 3.3). Quantitative analysis demonstrates that LDAMP SURE and LDAMP SURE-T achieved about 1.8 dB performance gain over BM3D-AMP (see Table 3.4), showing the best performance at higher sampling rates. However, at extremely low sampling ratio, our method slightly falls behind TVAL3. LDAMP SURE requires better data than BM3D-AMP reconstructed images from highly undersampled data to pretrain DnCNN. Therefore, one way to surpass TVAL3 at the highly undersampled case is to pretrain DnCNN with TVAL3 images.

Table 3.4: Average PSNRs (dB) and run times (sec) of 100 180x180 image reconstructions for CDP measurements case (no measurement noise) at various sampling rates ($M/N \times 100\%$).

Method	Training Time	$M/N = 5\%$		$M/N = 15\%$		$M/N = 25\%$	
		PSNR	Time	PSNR	Time	PSNR	Time
TVAL3 [30]	N/A	22.57	0.85	27.99	0.75	32.82	0.67
NLR-CS [32]	N/A	19.00	93.05	22.98	86.90	31.24	119.70
BM3D-AMP [51]	N/A	21.66	22.15	27.29	22.28	31.40	17.00
LDAMP BM3D	10.56 hrs	21.97	23.43	28.04	7.01	31.65	2.71
LDAMP BM3D-T	12.67 hrs	21.93	23.43	28.01	7.01	32.12	2.71
LDAMP SURE	15.22 hrs	22.18	23.43	29.14	7.01	33.26	2.71
LDAMP SURE-T	17.61 hrs	22.06	23.43	29.17	7.01	33.51	2.71
LDAMP MSE	10.17 hrs	22.12	23.43	28.87	7.01	33.88	2.71

Following the same steps as described in our paper, instead of using BM3D-AMP outputs, DnCNN was pre-trained with the TVAL3 reconstructed images (we denote this as LDAMP-TVAL3) and then was further trained using compressive sensing measurements using our proposed LDAMP SURE (we denote this as LDAMP SURE*). These results are reported in Table 3.5. In Table 3.4, LDAMP SURE was not able to outperform TVAL3 for CDP case when undersampled measurements were only $M/N = 5\%$. However, by using a different pre-trained network, the same proposed method surpassed all methods including TVAL3.

Table 3.5: Average PSNRs of 100 test images with 180×180 reconstructed for CDP at $M/N = 5\%$.

Methods	PSNR (dB)
TVAL3 [30]	22.57
NLR-CS [32]	19.00
BM3D-AMP [51]	21.66
LDAMP-TVAL3	22.72
LDAMP SURE*	22.88

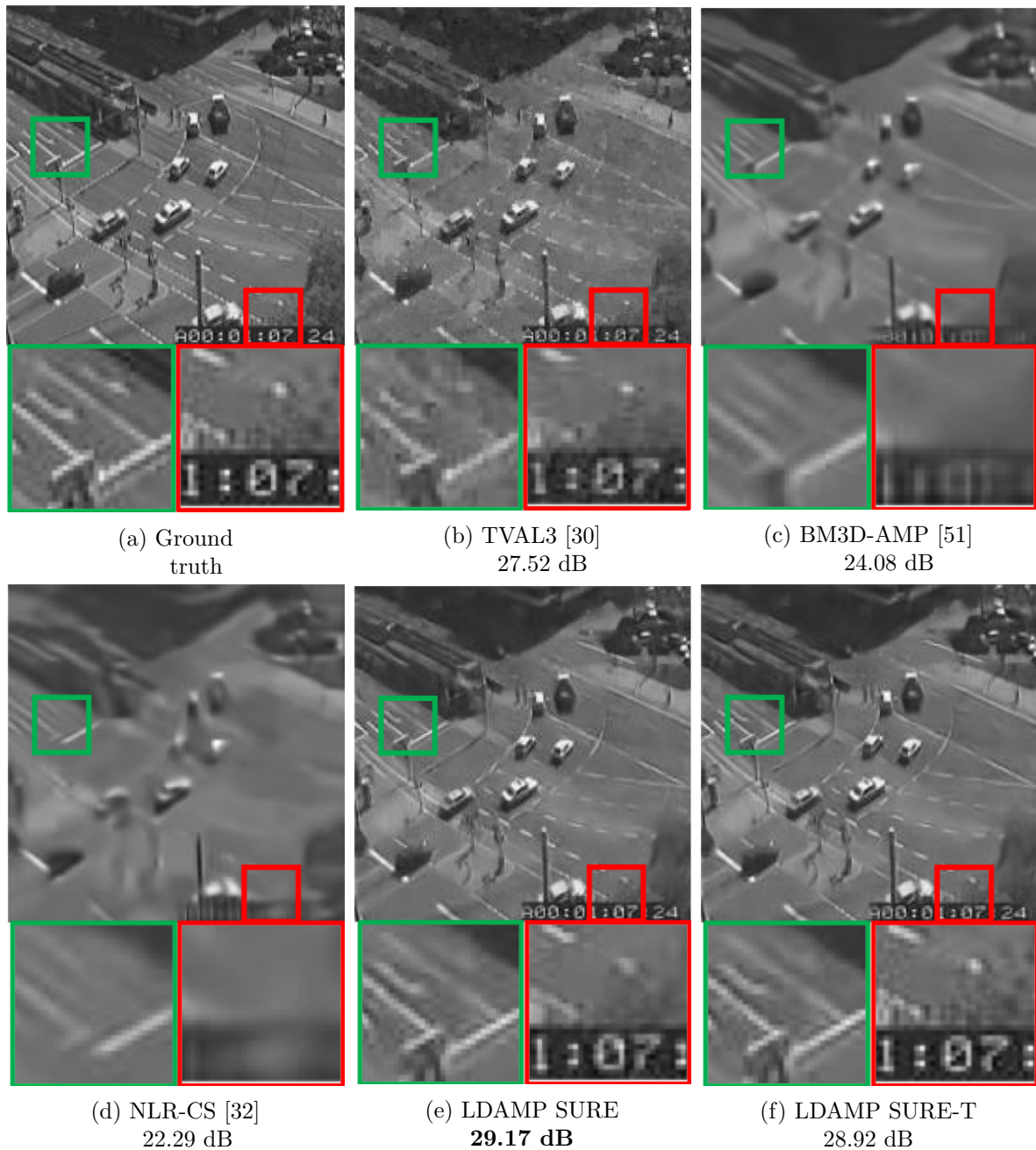


Figure 3.3: Reconstructions of 180×180 test image with CDP measurement matrix for $M/N = 0.15$ sampling rate.

3.2.2.3 CS MR measurement matrix

LDAMP SURE was applied to CS MRI reconstruction problem to demonstrate its generality and to show its performance on images that contain structures different from natural image dataset. We compared LDAMP SURE with state-of-the-art BM3D-AMP-MRI [34] for CS-MR image reconstruction along with TVAL3, BM3D-AMP, and dictionary learning based DL-MRI [3]. Average image recovery PSNRs and run times are tabulated in Table 3.6. The quantitative results demonstrate that proposed LDAMP SURE-T outperforms existing algorithms in all sampling ratios, yielding 0.15-0.33 dB gain over the second best reconstruction algorithm, BM3D-AMP-MRI.

Table 3.6: Average PSNRs (dB) and run times (sec) of 100 180x180 image reconstructions for CS-MRI measurements case (no measurement noise) at various sampling rates ($M/N \times 100\%$).

Method	Training Time	$M/N = 40\%$		$M/N = 50\%$		$M/N = 60\%$	
		PSNR	Time	PSNR	Time	PSNR	Time
TVAL3 [30]	N/A	36.76	0.58	37.13	0.24	38.35	0.21
DL-MRI [3]	N/A	36.60	98.51	37.81	97.58	39.13	99.44
BM3D-AMP-MRI [34]	N/A	37.42	14.76	38.94	15.00	40.51	15.36
BM3D-AMP [51]	N/A	36.15	96.23	36.29	84.34	39.53	98.01
LDAMP BM3D	9.31 hrs	37.12	6.26	38.63	6.14	39.53	6.10
LDAMP BM3D-T	12.41 hrs	37.65	6.26	38.92	6.14	39.87	6.10
LDAMP SURE	12.04 hrs	37.40	6.26	38.70	6.14	40.62	6.10
LDAMP SURE-T	16.05 hrs	37.77	6.26	39.09	6.14	40.71	6.10

Visual comparison analysis shows that proposed LDAMP SURE-T and BM3D-AMP-MRI produce high-quality reconstruction with almost no artifacts (see Figure 3.4). On the other hand, the residual error maps (red box) of TVAL3, BM3D-AMP, and DL-MRI clearly contain some structures, which indicates information loss in some image regions. Moreover, we can notice that BM3D-AMP reconstructed images are smoothed out, while proposed LDAMP SURE-T was able to preserve texture and fine details.

In sum, reconstruction results demonstrate that our proposed method yielded state-of-the-art performance, close to the ground truth.

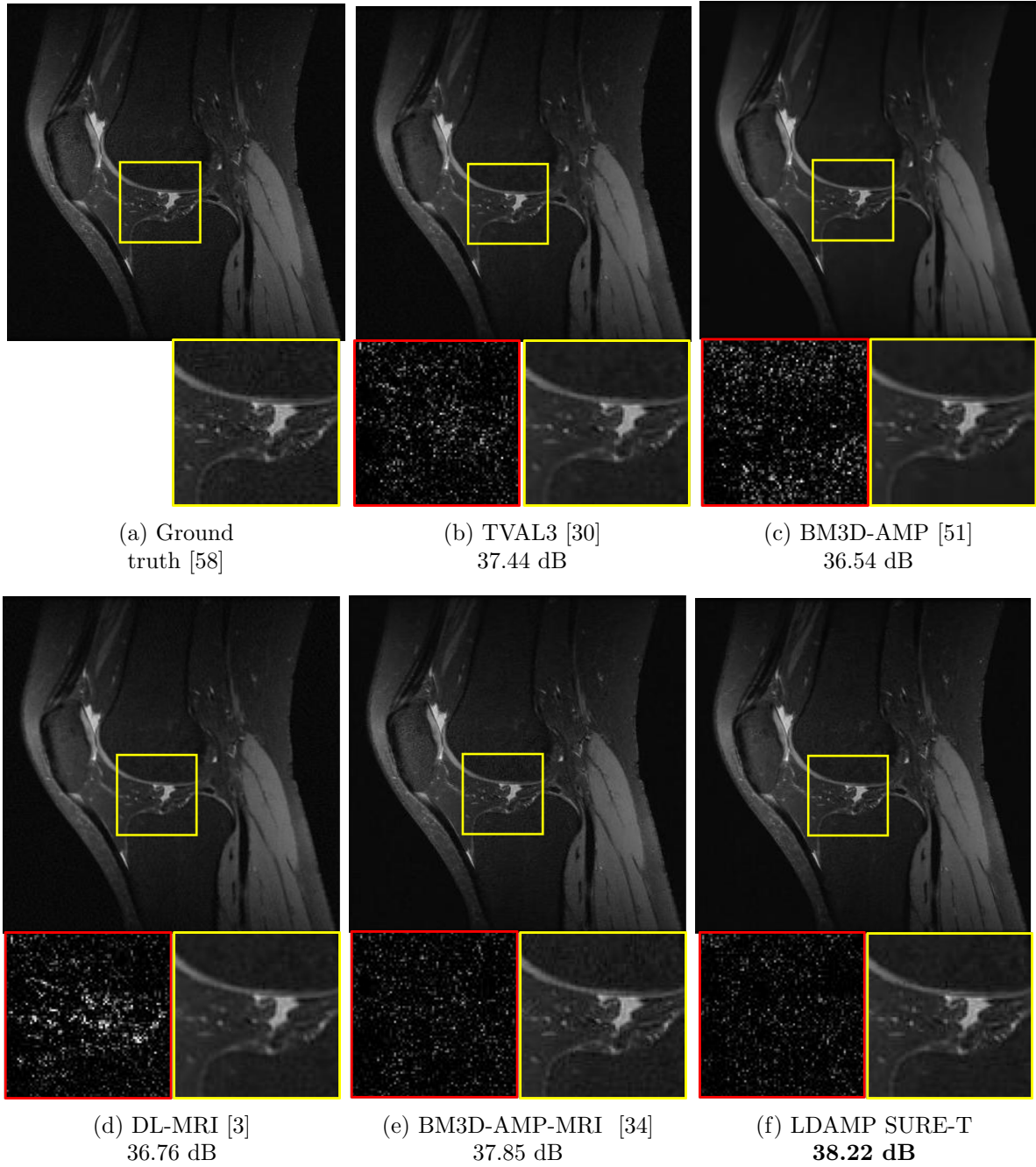


Figure 3.4: Reconstructions of 180×180 test image with CS-MRI measurement matrix for $M/N = 0.40$ sampling rate. Residual errors are shown in red boxes.

3.3 Extensions

3.3.1 Extension to a noisy measurement data

Noise in the measurement domain is an inevitable part of every compressed sensing system. Thus, in this part, we have conducted experiments with additive white Gaussian noise contaminated measurement data to imitate a more realistic case. Firstly, we generated noiseless measurements using *i.i.d.* Gaussian matrix and added AWGN noise with the -20dB signal to noise ratio (SNR):

$$SNR = -20 \times \log_{10} \frac{\|\mathbf{y}\|_2}{\|\boldsymbol{\epsilon}\|_2} \quad (\text{III.3})$$

Following the same procedures as described in Section 3.2.1, we obtained results for the proposed LDAMP SURE and LDAMP SURE-T (see Table 3.7). It is clear that our methods are advantageous over other unsupervised approaches in the presence of noise in the measurement domain. Moreover, we found that in highly undersampled case ($M/N = 5\%$) NLR-CS is more susceptible to the noise in measurements, while LDAMP SURE was more robust showing the best performance.

When we reconstruct highly undersampled noisy measurement test data, the performance of the pretrained network (LDAMP BM3D) and proposed LDAMP SURE was similar (0.05 dB difference), whereas at $M/N = 15\%$ sampling rate, MC-SURE trained network (LDAMP SURE) provided 0.2 dB performance gain over LDAMP BM3D. This indicates that undersampled measurements should have contained enough information to learn with MC-SURE and hence with higher quality measurement data, LDAMP SURE could gain more advantage.

Table 3.7: Average PSNRs (dB) and run times (sec) of 100 180x180 image reconstructions for Gaussian measurements case and observation noise with SNR = -20 dB at various sampling rates.

Method	$M/N = 5\%$		$M/N = 15\%$		$M/N = 25\%$	
	PSNR, dB	Time, sec	PSNR, dB	Time, sec	PSNR, dB	Time, sec
TVAL3 [30]	19.87	9.30	22.19	32.11	23.03	36.78
NLR-CS [32]	19.85	134.3	23.18	296.0	23.95	517.6
BM3D-AMP [51]	20.47	24.12	23.97	28.07	25.58	27.64
LDAMP BM3D	20.65	9.35	24.44	6.59	26.23	3.05
LDAMP BM3D-T	20.63	9.35	24.44	6.59	26.35	3.05
LDAMP SURE	20.70	9.35	24.63	6.59	26.38	3.05
LDAMP SURE-T	20.71	9.35	24.69	6.59	26.49	3.05
LDAMP MSE	20.91	9.35	24.67	6.59	26.47	3.05

3.3.2 Unsupervised fine-tuning using MC-SURE

Our proposed LDAMP SURE method does not require ground-truth images, therefore up to now, we have been using test measurement data for training LDAMP SURE-T. However, it is slow and less practical, since, for the future test data, one needs to retrain the network from scratch. Therefore, we propose a more convenient and faster method LDAMP SURE-FT, which also can take advantage of available test measurement data. LDAMP SURE-FT utilizes pretrained network parameters to fine-tune them on a test measurement data by minimizing MC-SURE.

The proposed fine-tuning process requires fixing the parameters of batch normalization in a pretrained denoiser. In our experiments, we took LDAMP SURE from Section 3.2.2.1 as a pretrained network for the fine-tuning process. Firstly, we reconstructed a single test image from measurement data with LDAMP SURE. Then, we estimated noise standard deviation and DnCNN denoiser was fine-tuned with MC-SURE on an individual noisy image (without patchifying) for 20 epochs with the learning rate of 10^{-4} and 50 epochs at 10^{-5} . Finally, fine-tuned DnCNN was used in LDAMP SURE-FT to reconstruct the image from its measurements. The fine-tuning process required around 20-25 seconds per 256×256 image, while reconstruction time is the same as for LDAMP SURE.

We evaluated the performance of proposed LDAMP SURE-FT as well as other methods on widely used 12 images (Set 12) with the size of 256×256 for various sampling ratios. Also, we included L-DAMP MSE performance for better comparison. Results of various methods are tabulated on Table 3.8. It is impressive that at $M/N = 0.25$ sampling rate, LDAMP SURE-FT has superior performance over other methods including LDAMP MSE on most of the test images and also on average. Proposed LDAMP SURE-FT was able to improve the performance over the LDAMP SURE on almost all of the test images, gaining 0.32dB on average. Such way of learning unique patterns and details inherent to each test image by the denoiser and hence tailoring the network for each test data allows LDAMP SURE-FT to effectively reconstruct images.

However, as the sampling rate decreases, we can observe that the performance of LDAMP SURE-FT degrades, finally making it inferior to LDAMP SURE at $M/N = 0.05$. Indeed, it is challenging to capture unique features from extremely undersampled data and consequently, LDAMP SURE-FT struggles to "overfit" the single test measurement data. In this case, it is more advantageous to use LDAMP SURE that utilizes priors from training measurement dataset.

Table 3.8: Results of image reconstruction methods on Set 12 (256×256) for various sampling rates (Performance in dB).

Image	C.Man	House	Peppers	Starfish	Monar.	F-16	Parrot	Lena	Barbara	Boat	Man	Couple	Average
Sampling rate: $M/N = 0.25$													
TVAL3 [30]	30.22	34.89	31.66	27.71	30.32	29.20	29.62	31.39	28.40	28.74	29.23	28.19	29.96
NLR-CS [32]	34.66	39.71	35.50	32.28	36.04	32.18	32.42	38.34	36.18	32.27	31.75	32.27	34.47
BM3D-AMP [51]	33.98	39.38	35.39	31.87	34.13	31.83	32.60	37.66	35.09	32.32	31.64	32.44	34.03
L-DAMP BM3D	32.45	37.92	35.74	33.80	36.39	32.58	32.52	38.40	32.37	33.67	32.71	33.53	34.34
L-DAMP SURE	33.32	38.51	35.88	34.28	36.91	32.90	32.83	38.67	32.53	33.80	32.98	33.67	34.69
L-DAMP SURE-FT	34.00	39.09	36.09	34.55	37.00	33.32	33.32	38.71	33.78	33.80	32.82	33.68	35.01
L-DAMP MSE	33.82	38.49	35.89	34.20	36.80	33.05	33.21	38.41	32.50	33.57	32.94	33.34	34.69
Sampling rate: $M/N = 0.15$													
TVAL3 [30]	27.07	32.45	27.92	24.79	26.35	25.39	26.53	28.54	26.27	26.17	26.80	25.74	27.00
NLR-CS [32]	30.41	37.03	32.90	28.84	31.67	28.67	29.30	34.41	32.01	28.78	28.72	28.83	30.96
BM3D-AMP [51]	30.52	37.03	32.55	28.59	30.52	28.29	29.56	33.98	31.56	28.87	28.72	28.85	30.75
L-DAMP BM3D	30.36	35.90	33.39	30.10	32.21	29.30	29.63	35.14	30.07	29.82	29.47	29.78	31.26
L-DAMP SURE	30.78	36.09	33.49	30.38	32.79	29.70	30.07	35.18	30.17	30.13	29.81	29.97	31.55
L-DAMP SURE-FT	31.25	36.52	33.41	30.88	32.97	29.63	30.35	35.18	30.68	30.00	29.59	29.75	31.68
L-DAMP MSE	31.21	36.38	33.63	30.62	33.09	29.91	30.46	35.19	30.25	30.11	29.90	29.97	31.73
Sampling rate: $M/N = 0.05$													
TVAL3 [30]	22.15	26.32	21.72	20.81	20.19	21.06	21.01	23.64	22.43	22.47	23.08	22.25	22.26
NLR-CS [32]	24.96	32.08	25.60	22.32	23.64	23.11	24.59	27.21	25.51	23.95	24.08	23.57	25.05
BM3D-AMP [51]	24.92	32.58	26.28	22.68	23.97	23.17	24.56	27.46	25.61	23.85	24.30	23.15	25.21
L-DAMP BM3D	25.93	32.63	26.92	22.76	25.29	23.65	25.27	27.99	25.76	24.28	24.65	23.75	25.74
L-DAMP SURE	26.23	32.64	27.19	22.82	25.51	23.82	25.41	28.25	25.83	24.46	24.81	23.87	25.90
L-DAMP SURE-FT	25.90	32.72	27.18	22.55	25.21	23.39	24.96	27.84	25.41	24.39	24.65	23.75	25.66
L-DAMP MSE	26.94	32.94	27.32	23.03	26.01	24.46	25.63	28.34	25.95	24.96	25.03	24.11	26.23

In sum, proposed LDAMP SURE-FT is a more practical way of utilizing test measurement data to reconstruct high-quality images in case of higher sampling rates. Moreover, our method yielded the best PSNR performance compared to all methods including LDAMP MSE for high sampling ratio.

CHAPTER IV

Conclusion

In this work, we proposed methods for unsupervised training of image denoisers with undersampled CS measurements. Our methods simultaneously performed CS image recovery and DNN denoiser learning. Our proposed method yielded better image quality than conventional methods at higher sampling rates for *i.i.d* Gaussian, CDP, and CS MR measurements. Thus, it may be possible that this work can be helpful for areas where obtaining ground truth images is challenging such as hyperspectral or medical imaging. Our proposed method can potentially be used with more advanced DNN denoisers for potentially better performance as far as they are trainable with MC-SURE loss [49].

We must point out that LDAMP SURE-T indeed requires additional training time with test set measurements. For large amount of test data, LDAMP SURE-T seems reasonable to use, but for a small amount of test data, LDAMP SURE-FT could be a better choice to minimize training time. Proposed LDAMP SURE-FT demonstrated superior performance over LDAMP SURE and was able to beat LDAMP MSE at higher sampling ratio. As shown in Table 3.8, using SURE-FT is less advantageous with lower sampling ratio possibly due to the lack of information in highly undersampled CS measurement. Training deep learning based image denoisers from undersampled training data still requires to contain enough information in the undersampled measurements. Only 5% of the full samples did not seem enough to achieve state-of-the-art performance possibly due to lack of information in the measurement. However, it seems that using a large number of highly undersampled measurements is beneficial to improve performance

since SURE-T achieved stat-of-the-art performance among all methods without ground truth data as shown in Tables 3.4 and 3.7.

There are some of the open directions that can be further explored and investigated in the near future. One of them is implementation of LDAMP SURE for color RGB image recovery. Dealing with compressively sampled measurements for each channel and applying our proposed method could potentially help to solve hyperspectral image reconstruction in an unsupervised way. Another open problem that needs attention is “clipping” in measurement domain, which is usually happening because of hardware limitations. In that case, measurement data is no longer contaminated with AWGN, but with clipped *i.i.d.* Gaussian noise. Moreover, in this work, we have conducted experiments with three different sensing matrices (Gaussian, CDP, undersampled Fourier), while there are plenty left (e.g. radon transform in CT imaging). This also can be one of the possible directions for our research.

References

- [1] Richard Baraniuk and Philippe Steeghs, “Compressive radar imaging,” in *2007 IEEE radar conference*. IEEE, 2007, pp. 128–133. iv, 1, 2
- [2] Michael Lustig, David Donoho, and John M Pauly, “Sparse MRI: The application of compressed sensing for rapid MR imaging,” *Magnetic Resonance in Medicine*, vol. 58, no. 6, pp. 1182–1195, 2007. 1, 5
- [3] Saiprasad Ravishankar and Yoram Bresler, “MR image reconstruction from highly under-sampled k-space data by dictionary learning,” *IEEE Transactions on Medical Imaging*, vol. 30, no. 5, pp. 1028–1041, 2011. 1, 5, 21, 22
- [4] Urs Gamper, Peter Boesiger, and Sebastian Kozerke, “Compressed sensing in dynamic mri,” *Magnetic Resonance in Medicine: An Official Journal of the International Society for Magnetic Resonance in Medicine*, vol. 59, no. 2, pp. 365–373, 2008. 1
- [5] Lee C Potter, Emre Ertin, Jason T Parker, and Müjdat Cetin, “Sparsity and Compressed Sensing in Radar Imaging,” *Proceedings of the IEEE*, vol. 98, no. 6, pp. 1006–1020, May 2010. 1
- [6] Marco F Duarte, Mark A Davenport, Dharmpal Takhar, Jason N Laska, Ting Sun, Kevin F Kelly, and Richard G Baraniuk, “Single-pixel imaging via compressive sampling,” *IEEE signal processing magazine*, vol. 25, no. 2, pp. 83–91, 2008. 1

REFERENCES

- [7] Florian Rousset, Nicolas Ducros, Andrea Farina, Gianluca Valentini, Cosimo D’Andrea, and Françoise Peyrin, “Adaptive basis scan by wavelet prediction for single-pixel imaging,” *IEEE Transactions on Computational Imaging*, vol. 3, no. 1, pp. 36–46, 2017. 1
- [8] Kihwan Choi, Jing Wang, Lei Zhu, Tae-Suk Suh, Stephen Boyd, and Lei Xing, “Compressed sensing based cone-beam computed tomography reconstruction with a first-order method,” *Medical Physics*, vol. 37, no. 9, pp. 5113–5125, Aug. 2010. 1
- [9] Lei Zhang, Wei Wei, Yanning Zhang, Fei Li, Chunhua Shen, and Qinfeng Shi, “Hyperspectral compressive sensing using manifold-structured sparsity prior,” in *IEEE International Conference on Computer Vision (ICCV)*, 2015, pp. 3550–3558. 1, 5
- [10] Lei Zhang, Wei Wei, Yanning Zhang, Chunna Tian, and Fei Li, “Reweighted Laplace prior based hyperspectral compressive sensing for unknown sparsity,” in *IEEE Conference on Computer Vision and Pattern Recognition (CVPR)*, 2015, pp. 2274–2281. 1, 5
- [11] Gonzalo R Arce, David J Brady, Lawrence Carin, Henry Arguello, and David S Kittle, “Compressive Coded Aperture Spectral Imaging: An Introduction,” *IEEE Signal Processing Magazine*, vol. 31, no. 1, pp. 105–115, Nov. 2013. 1
- [12] Roummel F Marcia, Zachary T Harmany, and Rebecca M Willett, “Compressive coded aperture imaging,” in *Computational Imaging VII*. International Society for Optics and Photonics, 2009, vol. 7246, p. 72460G. 1
- [13] Amir Beck and Marc Teboulle, “Gradient-based algorithms with applications to signal recovery,” *Convex optimization in signal processing and communications*, pp. 42–88, 2009. 1, 4
- [14] Amir Beck and Marc Teboulle, “A Fast Iterative Shrinkage-Thresholding Algorithm for Linear Inverse Problems,” *SIAM Journal on Imaging Sciences*, vol. 2, no. 1, pp. 183–202, Jan. 2009. 1, 4
- [15] E J Candes, J Romberg, and T Tao, “Robust uncertainty principles: exact signal reconstruction from highly incomplete frequency information,” *IEEE Transactions on Information Theory*, vol. 52, no. 2, pp. 489–509, Jan. 2006. 1, 4
- [16] D L Donoho, “Compressed sensing,” *IEEE Transactions on Information Theory*, vol. 52, no. 4, pp. 1289–1306, Mar. 2006. 1, 4

REFERENCES

- [17] Junfeng Yang and Yin Zhang, “Alternating Direction Algorithms for ℓ_1 -Problems in Compressive Sensing,” *SIAM Journal on Scientific Computing*, vol. 33, no. 1, pp. 250–278, Jan. 2011. 1, 4
- [18] Ender M Eksioğlu, “Decoupled algorithm for mri reconstruction using nonlocal block matching model: Bm3d-mri,” *Journal of Mathematical Imaging and Vision*, vol. 56, no. 3, pp. 430–440, 2016. 1
- [19] Karol Gregor and Yann LeCun, “Learning fast approximations of sparse coding,” in *International Conference on International Conference on Machine Learning (ICML)*, 2010, pp. 399–406. 1, 5, 8
- [20] Kyong Hwan Jin, Michael T McCann, Emmanuel Froustey, and Michael Unser, “Deep Convolutional Neural Network for Inverse Problems in Imaging,” *IEEE Transactions on Image Processing*, vol. 26, no. 9, pp. 4509–4522, Sept. 2017. 1, 5
- [21] Jian Zhang and Bernard Ghanem, “Ista-net: Interpretable optimization-inspired deep network for image compressive sensing,” in *Proceedings of the IEEE Conference on Computer Vision and Pattern Recognition*, 2018, pp. 1828–1837. 1
- [22] JH Rick Chang, Chun-Liang Li, Barnabas Póczos, BVK Vijaya Kumar, and Aswin C Sankaranarayanan, “One network to solve them all—solving linear inverse problems using deep projection models,” in *Proceedings of the IEEE International Conference on Computer Vision*, 2017, pp. 5888–5897. 1
- [23] Christopher A Metzler, Arian Maleki, and Richard G Baraniuk, “From denoising to compressed sensing,” *IEEE Transactions on Information Theory*, vol. 62, no. 9, pp. 5117–5144, 2016. 2, 5, 8, 11, 12, 14, 17
- [24] Yan Yang, Jian Sun, Huibin Li, and Zongben Xu, “Deep ADMM-Net for compressive sensing MRI,” in *Advances in Neural Information Processing Systems (NIPS)*, 2016, pp. 10–18. 2, 5
- [25] Harshit Gupta, Kyong Hwan Jin, Ha Q Nguyen, Michael T McCann, and Michael Unser, “CNN-Based Projected Gradient Descent for Consistent CT Image Reconstruction,” *IEEE transactions on medical imaging*, pp. 1–1, May 2018. 2, 5
- [26] Christopher A Metzler, Arian Maleki, and Richard G Baraniuk, “Learned D-AMP: Principled neural network based compressive image recovery,” in *Advances in Neural Information Processing Systems (NIPS)*, 2017, pp. 1770–1781. 2, 3, 5, 7, 8, 10, 11, 12, 14

REFERENCES

- [27] Shakarim Soltanayev and Se Young Chun, “Training and refining deep learning based denoisers without ground truth data,” *CoRR*, vol. abs/1803.01314, no. 1803.01314, 2019. 3
- [28] Magaiya Zhussip, Shakarim Soltanayev, and Se Young Chun, “Training deep learning based image denoisers from undersampled measurements without ground truth and without image prior,” *IEEE Conference on Computer Vision and Pattern Recognition, Accepted*, 2019. 3
- [29] D L Donoho, A Maleki, and A Montanari, “Message-passing algorithms for compressed sensing,” *Proceedings of the National Academy of Sciences (PNAS)*, vol. 106, no. 45, pp. 18914–18919, Nov. 2009. 4
- [30] Chengbo Li, Wotao Yin, and Yin Zhang, “User’s guide for TVAL3: TV minimization by augmented Lagrangian and alternating direction algorithms,” *CAAM report*, vol. 20, no. 46-47, pp. 4, 2009. 5, 17, 18, 19, 20, 21, 22, 23, 25
- [31] Xin Yuan, Patrick Llull, Xuejun Liao, Jianbo Yang, David J Brady, Guillermo Sapiro, and Lawrence Carin, “Low-cost compressive sensing for color video and depth,” in *IEEE Conference on Computer Vision and Pattern Recognition (CVPR)*, 2014, pp. 3318–25. 5
- [32] Weisheng Dong, Guangming Shi, Xin Li, Yi Ma, and Feng Huang, “Compressive sensing via nonlocal low-rank regularization,” *IEEE Transactions on Image Processing*, vol. 23, no. 8, pp. 3618–3632, 2014. 5, 17, 18, 19, 20, 23, 25
- [33] Kostadin Dabov, Alessandro Foi, Vladimir Katkovnik, and Karen Egiazarian, “Image denoising by sparse 3-d transform-domain collaborative filtering,” *IEEE Transactions on Image Processing*, vol. 16, no. 8, pp. 2080–2095, 2007. 5, 7, 8
- [34] Ender M Eksioğlu and A Korhan Tanc, “Denoising AMP for MRI reconstruction: BM3D-AMP-MRI,” *SIAM Journal on Imaging Sciences*, vol. 11, no. 3, pp. 2090–2109, 2018. 5, 16, 21, 22
- [35] Yann LeCun, Yoshua Bengio, and Geoffrey Hinton, “Deep learning.,” *Nature*, vol. 521, no. 7553, pp. 436–444, May 2015. 5
- [36] Harold C Burger, Christian J Schuler, and Stefan Harmeling, “Image denoising: Can plain neural networks compete with BM3D?,” in *IEEE Conference on Computer Vision and Pattern Recognition (CVPR)*, 2012, pp. 2392–2399. 5, 8

REFERENCES

- [37] Viren Jain and Sebastian Seung, “Natural image denoising with convolutional networks,” in *Advances in Neural Information Processing Systems (NIPS)*, 2009, pp. 769–776. 5, 8
- [38] Pascal Vincent, Hugo Larochelle, Isabelle Lajoie, Yoshua Bengio, and Pierre Antoine Manzagol, “Stacked denoising autoencoders: Learning Useful Representations in a Deep Network with a Local Denoising Criterion,” *Journal of Machine Learning Research*, vol. 11, pp. 3371–3408, Dec. 2010. 5, 8
- [39] Junyuan Xie, Linli Xu, and Enhong Chen, “Image denoising and inpainting with deep neural networks,” in *Advances in Neural Information Processing Systems (NIPS)*, 2012, pp. 341–349. 5, 8
- [40] Kai Zhang, Wangmeng Zuo, Yunjin Chen, Deyu Meng, and Lei Zhang, “Beyond a Gaussian denoiser: Residual learning of deep CNN for image denoising,” *IEEE Transactions on Image Processing*, vol. 26, no. 7, pp. 3142–3155, 2017. 5, 8
- [41] Dongwon Park, Kwanyoung Kim, and Se Young Chun, “Efficient module based single image super resolution for multiple problems,” in *IEEE Conference on Computer Vision and Pattern Recognition (CVPR) Workshops*, 2018, pp. 995–1003. 5, 8
- [42] Kerstin Hammernik, Teresa Klatzer, Erich Kobler, Michael P Recht, Daniel K Sodickson, Thomas Pock, and Florian Knoll, “Learning a variational network for reconstruction of accelerated MRI data,” *Magnetic Resonance in Medicine*, vol. 79, no. 6, pp. 3055–3071, Nov. 2017. 5
- [43] Kuldeep Kulkarni, Suhas Lohit, Pavan K Turaga, Ronan Kerviche, and Amit Ashok, “ReconNet: Non-iterative reconstruction of images from compressively sensed measurements,” in *IEEE Conference on Computer Vision and Pattern Recognition (CVPR)*, 2016, pp. 449–458. 5
- [44] Kai Xu, Zhikang Zhang, and Fengbo Ren, “LAPRAN: A scalable Laplacian pyramid reconstructive adversarial network for flexible compressive sensing reconstruction,” in *European Conference on Computer Vision (ECCV)*, 2018, pp. 491–507. 5
- [45] Jian Zhang and Bernard Ghanem, “ISTA-Net: Interpretable optimization-inspired deep network for image compressive sensing,” in *IEEE Conference on Computer Vision and Pattern Recognition (CVPR)*, 2018, pp. 1828–1837. 5
- [46] Ashish Bora, Ajil Jalal, Eric Price, and Alexandros G Dimakis, “Compressed sensing using generative models,” in *International Conference on Machine Learning (ICML)*, 2017, pp. 537–46. 5, 6

REFERENCES

- [47] Jaakko Lehtinen, Jacob Munkberg, Jon Hasselgren, Samuli Laine, Tero Karras, Miika Aittala, and Timo Aila, “Noise2Noise: Learning image restoration without clean data,” in *International Conference on Machine Learning (ICML)*, 2018, pp. 2965–74. 6
- [48] A Bora, E Price, and A G Dimakis, “AmbientGAN: Generative models from lossy measurements,” in *International Conference on Learning Representations (ICLR)*, 2018. 6
- [49] Shakarim Soltanayev and Se Young Chun, “Training deep learning based denoisers without ground truth data,” in *Advances in Neural Information Processing Systems (NIPS)*, 2018. 6, 9, 11, 16, 26
- [50] C. Metzler, A. Mousavi, R. Heckel, and R. Baraniuk, “Unsupervised learning with stein’s unbiased risk estimator,” in *International Biomedical and Astronomical Signal Processing Frontiers workshop*, 2019. 6
- [51] Christopher A Metzler, Arian Maleki, and Richard G Baraniuk, “BM3D-AMP: A new image recovery algorithm based on BM3D denoising,” in *IEEE International Conference on Image Processing (ICIP)*, 2015, pp. 3116–3120. 7, 14, 17, 18, 19, 20, 21, 22, 23, 25
- [52] Sathish Ramani, Thierry Blu, and Michael Unser, “Monte-Carlo SURE: A black-box optimization of regularization parameters for general denoising algorithms,” *IEEE Transactions on Image Processing*, vol. 17, no. 9, pp. 1540–1554, 2008. 7
- [53] Mark Borgerding, Philip Schniter, and Sundeep Rangan, “AMP-inspired deep networks for sparse linear inverse problems,” *IEEE Transactions on Signal Processing*, vol. 65, no. 16, pp. 4293–4308, 2017. 8
- [54] Antoni Buades, Bartomeu Coll, and Jean-Michel Morel, “A non-local algorithm for image denoising,” in *IEEE Conference on Computer Vision and Pattern Recognition (CVPR)*, 2005, pp. 60–65. 8
- [55] Minh Phuong Nguyen and Se Young Chun, “Bounded Self-Weights Estimation Method for Non-Local Means Image Denoising Using Minimax Estimators,” *IEEE Transactions on Image Processing*, vol. 26, no. 4, pp. 1637–1649, Feb. 2017. 8
- [56] Eirikur Agustsson and Radu Timofte, “NTIRE 2017 challenge on single image super-resolution: Dataset and study,” in *IEEE Conference on Computer Vision and Pattern Recognition Workshop (CVPRW)*, 2017. 15, 18

REFERENCES

- [57] D. Martin, C. Fowlkes, D. Tal, and J. Malik, “A database of human segmented natural images and its application to evaluating segmentation algorithms and measuring ecological statistics,” in *IEEE International Conference on Computer Vision (ICCV)*, July 2001, vol. 2, pp. 416–423. 15
- [58] Kevin Epperson, Anne Marie Sawyer, Michael Lustig, Marcus Alley, Martin Uecker, Patrick Virtue, Peng Lai, and Shreyas Vasanawala, “Creation of Fully Sampled MR Data Repository for Compressed Sensing of the Knee,” in *SMRT Conference*, 2013. 15, 22
- [59] Diederik P. Kingma and Jimmy Lei Ba, “ADAM: A method for stochastic optimization,” in *International Conference on Learning Representations (ICLR)*, 2015. 15, 16
- [60] Charles-Alban Deledalle, Samuel Vaiter, Jalal Fadili, and Gabriel Peyré, “Stein Unbiased GrAdient estimator of the Risk (SUGAR) for multiple parameter selection,” *SIAM Journal on Imaging Sciences*, vol. 7, no. 4, pp. 2448–2487, 2014. 16
- [61] Emmanuel J Candes, Xiaodong Li, and Mahdi Soltanolkotabi, “Phase retrieval from coded diffraction patterns,” *Applied and Computational Harmonic Analysis*, vol. 39, no. 2, pp. 277–299, 2015. 19